

Cubic anomalies in WMAP

Kate Land and João Magueijo ^{*}

Theoretical Physics Group, Imperial College, Prince Consort Road, London SW7 2BZ, UK

4 June 2018

ABSTRACT

We perform a frequentist analysis of the bispectrum of WMAP first year data. We find clear signal domination up to $\ell \approx 200$, with overall consistency with Gaussianity, except for the following features. There is a flat patch (i.e. a low χ^2 region) in the same- ℓ components of the bispectrum spanning the range $\ell = 32 - 62$; this *may be* interpreted as ruling out Gaussianity at the 99.6% confidence level. There is also an asymmetry between the North and South inter- ℓ bispectrum components at the 99% confidence level. The preferred asymmetry axis correlates well with the $(\ell, b) = (57, 10)$ direction quoted in the literature for asymmetries in the power spectrum and three-point correlation function. However our analysis of the quadrupole (its bispectrum and principal axes) fails to make contact with previously claimed anomalies.

Key words: Cosmic microwave background - Gaussianity tests.

1 INTRODUCTION

The hypothesis of statistical Gaussianity plays a central role in the standard theory of structure formation. Unsurprisingly, a large amount of effort has gone into checking this assumption, with the cosmic microwave background (CMB) anisotropy being its cleanest probe. The early work on COBE-DMR data was punctuated by the first findings that we might not live in the best of all possible worlds. The data passed standard, but not very discriminative Gaussianity tests (Kogut et al 1996). Upon closer inspection, however, anomalies were discovered (Ferreira, Magueijo & Górski 1998; Novikov, Feldman and Shandarin 1998). For example, the bispectrum analysis of the 4-year dataset revealed evidence against Gaussianity (Ferreira, Magueijo & Górski 1998; Magueijo 2000) to a high significance level.

The possibility remained that these non-Gaussianity “detections” might be due to undocumented systematic errors. This hope was partly satisfied by the discovery of subtle errors in the map-making procedure of COBE-DMR (Banday, Zaroubi & Górski 1999). Pixelization artifacts and further systematic errors in COBE were later found, with the aid of the higher quality WMAP data (Magueijo & Medeiros 2003). Indeed all the early work was plagued by high noise levels, poor resolution and the threat of multiple systematics. The WMAP project (Bennett & al 2003a) has opened up the doors for the first convincing evaluation of the hypothesis of Gaussianity.

Ironically the WMAP data has renewed con-

cerns over the Gaussianity of the CMB fluctuations (Copi, Huterer & Starkman 2003; Eriksen & al 2004b; Coles & al 2003; Cruz & al 2003; Hansen & al 2004; Hansen, Banday & Górski 2004; Vielva & al 2003; Komatsu, Spergel & Wandelt 2003; Park 2003; Larson & Wandelt 2004; Mukherjee & Wang 2004; Eriksen & al 2004a; Schwarz & al 2004). Most worryingly, it appears that the data displays a North-South asymmetry in the power spectrum and three-point correlation function. This questions both the statistical isotropy and Gaussianity of the data. The spread in power spectrum and 3-point function is sensitive to the fourth and sixth momenta of the distribution.

In this paper we perform a frequentist analysis of the WMAP bispectrum. This is to be contrasted with the work of Komatsu & al (2003), where the WMAP bispectrum is analysed with reference to a particular non-Gaussian model, parameterised by the non-linear coupling parameter f_{NL} . Such work neglects bispectrum non-Gaussianity that might arise in any other theory; or indeed that might be due to spurious systematics. Our exploratory approach is to be seen as complementary to that by Komatsu & al (2003). In particular we shall be concerned with correlating our bispectrum studies and the WMAP anomalies found by other groups, namely claims for North-South irregularities.

Our paper is organised as follows. In Section 2 we establish our notation and bispectrum definitions. We introduce same- ℓ and inter- ℓ normalised bispectrum measures, denoted by I_ℓ and J_ℓ respectively. These are sensitive to phase correlations within a single multipole and between adjacent multipoles. Their normalisation ensures that for a

^{*} E-mail:kate.land@imperial.ac.uk,j.magueijo@ic.ac.uk

Gaussian process they are statistically independent from the power spectrum (Magueijo 1995).

In Section 3 we then evaluate I_ℓ and J_ℓ for WMAP and compare results with Monte-Carlo simulations in which a Gaussian signal is subject to the same noise and beam characteristics as the real data. We also discuss various galactic masks. We find a low χ^2 region in the I_ℓ in the range $\ell = 32 - 62$. Depending on the prior, this may be interpreted as ruling out Gaussianity at the 99.6% confidence level (we relegate to Section 6 a discussion of possible selection effects).

In Section 4 we re-examine claims for North-South asymmetries in CMB from the point of view of the bispectrum. We find asymmetries in the inter- ℓ components of the bispectrum which are not only statistically significant (99% confidence level, *even when all possible selection effects are taken into account*), but also correlates well with the $(\ell, b) = (57, 10)$ direction quoted in the literature. Our detection is independent from, but reinforces similar anomalies found for the 3-point correlation function (Eriksen & al 2004a).

However, our analysis of the quadrupole fails to make contact with previously claimed weird features. In Section 5 we provide a geometrical interpretation of the quadrupole where the bispectrum may be seen as a shape factor. In addition we identify three orthogonal principal directions. None of these show anything abnormal or correlate with suspicious directions.

In Section 7 we conclude with a summary of our findings.

2 THE BISPECTRUM

We start by reviewing some results and definitions pertaining to the bispectrum. Given a full-sky map, $\frac{\Delta T}{T}(\mathbf{n})$, this may be expanded into Spherical Harmonic functions:

$$\frac{\Delta T}{T}(\mathbf{n}) = \sum_{\ell} \delta T_{\ell} = \sum_{\ell m} a_{\ell m} Y_{\ell m}(\mathbf{n}) \quad (1)$$

Each multipole component δT_{ℓ} contains fluctuations with a characteristic angular scale inversely proportional to ℓ . The coefficients $a_{\ell m}$ are not rotationally invariant but may be combined into rotationally invariant multilinear forms (see Magueijo, Ferreira & Górski (1998) for a possible algorithm). The only *bilinear* invariant is the commonly used angular power spectrum, given by $\hat{C}_{\ell} = \frac{1}{2\ell+1} \sum_m |a_{\ell m}|^2$. This gives a measure of the overall intensity of each multipole. The most general *cubic* invariant is the bispectrum, and is given by

$$\hat{B}_{\ell_1 \ell_2 \ell_3} = \frac{\begin{pmatrix} \ell_1 & \ell_2 & \ell_3 \\ 0 & 0 & 0 \end{pmatrix}^{-1}}{(2\ell_1 + 1)^{\frac{1}{2}} (2\ell_2 + 1)^{\frac{1}{2}} (2\ell_3 + 1)^{\frac{1}{2}}} \times \sum_{m_1 m_2 m_3} \begin{pmatrix} \ell_1 & \ell_2 & \ell_3 \\ m_1 & m_2 & m_3 \end{pmatrix} a_{\ell_1 m_1} a_{\ell_2 m_2} a_{\ell_3 m_3} \quad (2)$$

where the (...) is the Wigner $3J$ symbol. The proportionality constant is chosen so as to enforce a roughly constant cosmic variance. There are various alternative ways in which the bispectrum may be computed; for instance

$$\hat{B}_{\ell_1 \ell_2 \ell_3} \propto \int d\Omega \delta T_{\ell_1} \delta T_{\ell_2} \delta T_{\ell_3} \quad (3)$$

with similar constructions for higher order moments (Spergel & Goldberg 1999; Komatsu & al 2002). This may be computationally advantageous.

Selection rules require that $\ell_1 + \ell_2 + \ell_3$ be even, and we impose $\ell_i \geq 2$. So for even ℓ the choice $\ell_1 = \ell_2 = \ell_3 = \ell$ leads to the “single- ℓ ” bispectrum $\hat{B}_{\ell} = B_{\ell \ell \ell}$ (Ferreira, Magueijo & Górski 1998). Other bispectrum components are sensitive to correlations between different scales. The simplest chain of correlators is therefore $\hat{A}_{\ell} = B_{\ell-1 \ell \ell+1}$ – the “inter- ℓ ” bispectrum (Magueijo 2000). Other components, involving more distant multipoles, may be considered (Sandvik & Magueijo 2001) but they are very likely to be dominated by noise; it has been observed that non-Gaussian inter-scale correlations decay with ℓ separation.

In this paper we shall consider ratios

$$I_{\ell}^3 = \frac{\hat{B}_{\ell}}{(\hat{C}_{\ell})^{3/2}} \quad (4)$$

and

$$J_{\ell}^3 = \frac{\hat{A}_{\ell}}{(\hat{C}_{\ell-1})^{1/2} (\hat{C}_{\ell})^{1/2} (\hat{C}_{\ell+1})^{1/2}} \quad (5)$$

These quantities are invariant under rotations and parity; they are also dimensionless and therefore less dependent upon the power spectrum. Indeed for a Gaussian process it may be proved (Magueijo 1995) that it is this normalised – and not the un-normalized – bispectrum that is statistically independent from the power spectrum. This matter will be very important later when we compare previously found North/South power spectrum asymmetries with asymmetries found in the normalised bispectrum.

3 THE WMAP BISPECTRUM

The WMAP mission (Bennett & al 2003a) produced full sky CMB maps from ten differencing assemblies (DAs); four in the W band (94 GHz), two V band (61 GHz), two Q band (41 GHz), one Ka band (33 GHz), and one K band (23 GHz). The K and Ka bands are dominated by galactic emission and therefore neglected for cosmological analysis. We use the “foreground cleaned” maps¹, where the Galactic foreground signal, consisting of synchrotron, free-free, and dust emission, was removed using the 3-band, 5-parameter template fitting method described in Bennett & al (2003b). All maps are rendered using the HEALPix² package (Górski, Hivon & Wandelt 1998), with pixelization level nside=512.

We examined the bispectrum of an “inverse-noise-squared” coadded map based on the Q, V and W bands, that is a map:

$$T(n) = \frac{\sum_{i=3}^{10} T_i(n)/\sigma_i^2}{\sum_{i=3}^{10} 1/\sigma_i^2} \quad (6)$$

¹ Publicly available from <http://lambda.gsfc.nasa.gov>

² <http://www.eso.org/science/healpix/index.html>

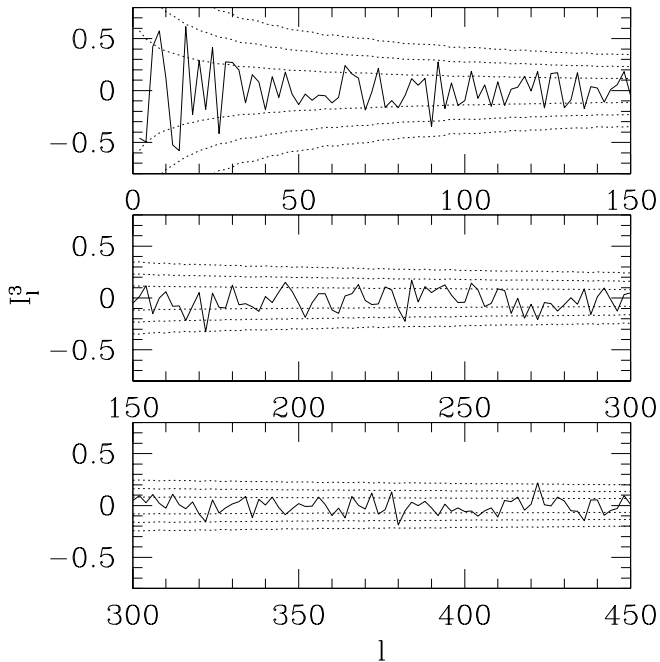


Figure 1. The WMAP single- ℓ bispectrum for a coadded map with the Kp0 mask. We have superposed the 1, 2, and 3 sigma error bars inferred from Gaussian simulations.

where

$$1/\sigma_i^2 = \sum_{n=1}^{N_{pix}} 1/\sigma_i^2(n) \quad , \quad \sigma_i^2(n) = \sigma_{0,i}^2/N_{obs_i}(n)$$

where T_i is the sky map for the DA i with the foreground galactic signal subtracted, and $\sigma_{0,i}^2$ is the noise per observation for DA i , whose values are given by Bennett & al (2003a). We apply the Kp0 mask to this map (Bennett & al 2003b) to cut possible remaining galactic contamination near the disk, and then we remove any residual monopole.

In Figs. 1 and 2 we plot the I_ℓ^3 and J_ℓ^3 bispectrum components, for $\ell = 2 - 450$, and $\ell = 4 - 450$ respectively, for the WMAP first year coadded map with a Kp0 mask. We compare these results with those from Monte Carlo simulations of Gaussian maps with the same noise and beam characteristics as the WMAP instrument, and subject to the Kp0 mask. From 5,000 sky realizations we inferred the 1, 2, and 3-sigma variance lines, also plotted in Figs. 1 and 2.

Before we apply a goodness of fit statistic to these results it is important to select a signal dominated ℓ range. This should be estimated from *real* data; any other algorithms risk including noise-dominated multipoles into the analysis, thus ending up testing the Gaussianity of noise. Such a direct estimate may be obtained by evaluating I_ℓ^3 and J_ℓ^3 for the different channels. The noise in each of these bands is uncorrelated, so the impact of the noise upon the statistics may be inferred from the dispersion from channel to channel. As can be seen in Figs. 3 and 4 the bispectrum is signal dominated up to $\ell \approx 200$.

Bearing this in mind we may now compute the reduced chi-squared for a selection of signal dominated sections in ℓ space. Table 1 records the fraction of simulations that found a lower χ^2 value for the indicated ℓ range (note that the ℓ

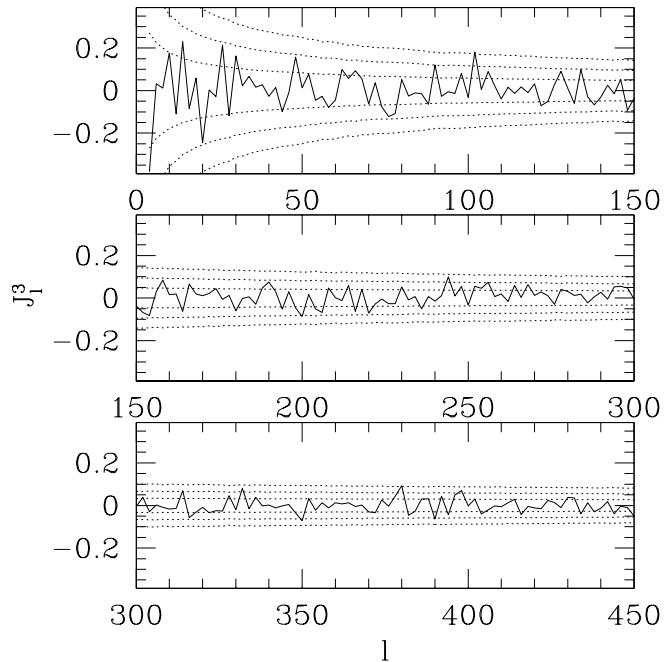


Figure 2. The WMAP inter- ℓ bispectrum for a coadded map with the Kp0 mask. We have superposed the 1, 2, and 3 sigma error bars inferred from Gaussian simulations.

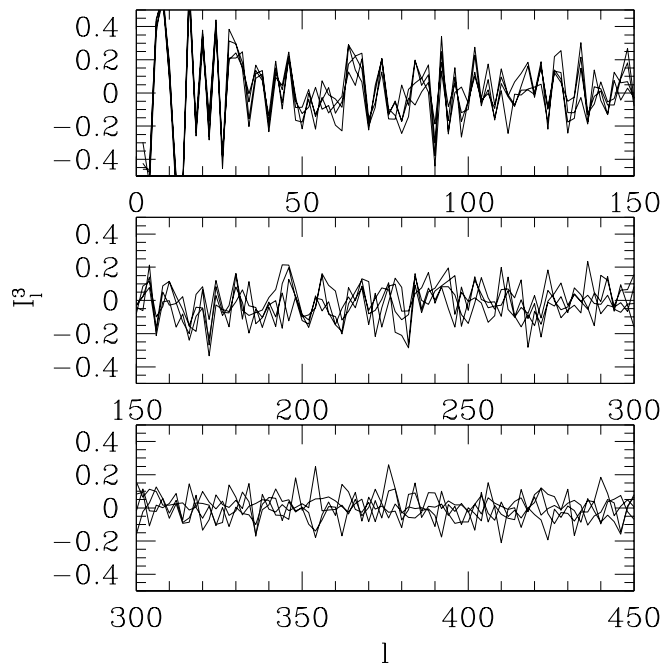


Figure 3. The WMAP single- ℓ bispectrum for the channels that most contribute to the coadded map (Q1, Q2, V1 and V2).

range can start at $\ell = 4$ for J_ℓ and at $\ell = 2$ for I_ℓ). We find the WMAP J_ℓ^3 consistent with Gaussianity. However, for the I_ℓ^3 we observe a long “flat patch”: a region where all points are within 1 sigma. Our “flat patch” covers points $\ell = 32 - 62$ inclusively, as can be seen in Fig. 1. For this range we would expect a low χ^2 value, and at 0.329 it is smaller than 99.6%

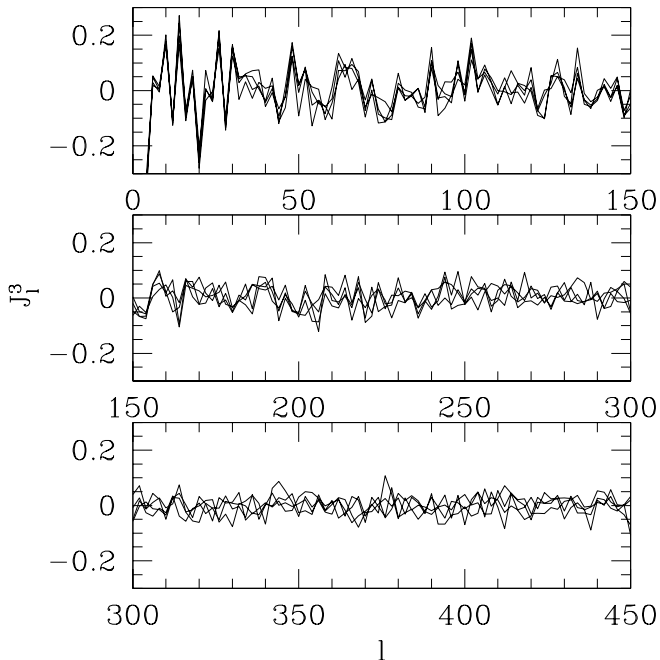


Figure 4. The WMAP inter- ℓ bispectrum for the channels that most contribute to the coadded map (Q1, Q2, V1 and V2).

Table 1. The fraction of our simulations that found a lower χ^2

l range	J_ℓ^3	I_ℓ^3
2(4)-200	0.75	0.62
2(4)-100	0.48	0.58
2(4)-50	0.466	0.617
30-70	0.239	0.033
32-62	0.141	0.004
50-100	0.409	0.437
76-126	0.758	0.642
100-150	0.854	0.445
126-176	0.79	0.82
150-200	0.746	0.617

of those from simulations for this range. Critically we need to take account of selection effects, and so by letting each simulation pick out its longest “flat patch” within $\ell = 2-300$ we can account for the fact that we have honed into the most significant region. We find that a “flat patch” of this length or longer appears in 8.8% of the simulations. Further, a χ^2 of 0.329 is not at all significant for a “flat patch” the same length as ours: 67.7% having an even lower χ^2 . Of course the last conclusion depends on whether or not a prior exists which makes the range $\ell = 32 - 62$ special. If such a prior exists then we have rejected Gaussianity at a high level of confidence. We shall return to this matter in Section 6.

It is important to evaluate the impact of the galactic cut on these conclusions. We note that the ILC map (Bennett & al 2003a) also displays this “flat patch”, but only when the central galactic area is masked. The ILC map does not completely avoid foreground emissions, and so the galactic region will display non-Gaussian signals. When the ILC map is not masked, it is this galactic emission that di-

lutes our “flat patch”. For both maps the “flat patch” does not diminish as we increase the masked region, implying that the “flat patch” is not due to galactic emission.

We conclude that the the normalised inter- ℓ and single- ℓ bispectrum from the whole sky are consistent with Gaussianity.

4 HEMISPHERE ASYMMETRIES IN THE BISPECTRUM

Recently there have been numerous detections of asymmetry in the CMB (e.g., Copi, Huterer & Starkman (2003); Coles & al (2003); Eriksen & al (2004b); Hansen & al (2004); Hansen, Banday & Górski (2004); Eriksen & al (2004a); Schwarz & al (2004)). Specifically, Eriksen & al (2004a) found a significant lack of power and a surprisingly featureless pseudo collapsed 3-point correlation function, $C^{(3)}(\theta)$, in the Northern ecliptic hemisphere. The asymmetry in the power spectrum was maximised for a North pole at approximately $(\ell, b) = (57, 10)$ ³. The non-normalised bispectrum is related to the Legendre transform of $C^{(3)}(\theta)$. Therefore by observing the I_ℓ^3 and J_ℓ^3 on different hemispheres we can probe any ℓ dependence of the $C^{(3)}(\theta)$ asymmetry. We emphasise that these will also be independent of the power spectrum for a Gaussian field (see Magueijo (1995) for an analytical proof for $\ell = 2$).

4.1 Inter- ℓ normalised bispectrum

We calculate the J_ℓ^3 on the Northern and Southern hemispheres for a North pole at $(\ell, b) = (57, 10)$. In Fig. 5 we plot them against each other, and against the whole sky results. We also plot the 1 sigma variance lines for the whole sky (the spread is a little wider for a half-sky). We notice that the Northern results appear to take higher values than the Southern. For 34 of the 49 points the Northern result is higher, and when it is not the difference is small. We note that the individual χ^2 values do not reveal any significant departure from Gaussianity for either the Northern or Southern results. It is the difference between the hemispheres that is significant.

We quantify this feature by measuring the sum of the differences:

$$K = \sum_{\ell} \frac{J_{\ell,N}^3 - J_{\ell,S}^3}{\sigma_{\ell}} \quad (7)$$

We calculate K for a North pole at (57,10), and at the ecliptic North pole position (96,30), and at a further 53 positions uniformly distributed in the Northern galactic hemisphere. We infer the value of K for the opposite North pole positions, in the Southern galactic hemisphere. We then perform Gaussian Monte Carlo simulations, as above, in order to evaluate the statistical significance of the observed WMAP asymmetry. For each simulation we allow the North pole to vary over the same positions and we record the maximum $|K|$ value seen in each simulation.

³ Galactic coordinates: Longitude $\ell \in [-180(E), +180(W)]$, Latitude $b \in [-90(S), +90(N)]$, with $(\ell, b) = (0, 0)$ towards the galactic centre.

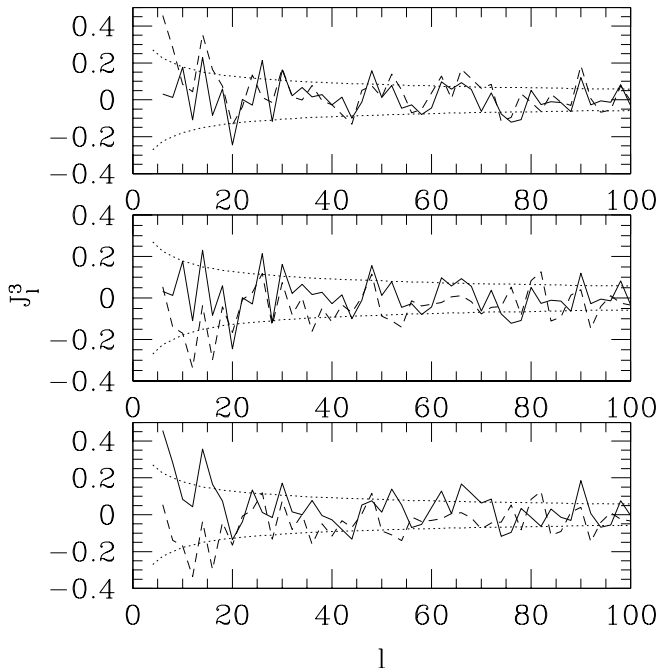


Figure 5. The J_ℓ^3 spectra: top panel, allsky (bold) and Northern (dashed); middle panel, allsky (bold) and Southern (dashed); bottom panel, Northern (bold) and Southern (dashed).

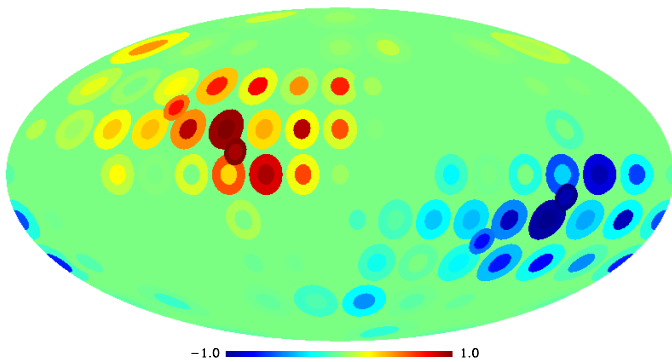


Figure 6. Asymmetry in the J_ℓ^3 as measured by $|K|$. At each North pole position we show the fraction of simulations with a lower $|K|_{max}$ value, multiplied by the \pm sign of the K_{WMAP} result. Results are also shown for North pole position (57,10) and its opposite (-123,-10), and for the ecliptic poles.

Figure 6 plots, at the corresponding North pole position, the fraction of simulations with a lower $|K|_{max}$ value than the $|K_{WMAP}|$ value from that North pole. This fraction is then displayed with the \pm sign of this K_{WMAP} result *i.e.* -1, and +1 indicates a North pole position returning higher asymmetry than all the simulations. We show the results for the ranges $\ell = 4-100$ (larger circles), and $\ell = 4-50$ (smaller circles).

In Table 2 we list the results for the three North pole positions that find the maximum value of K , for WMAP. We also show the fraction of simulations that return a lower $|K|_{max}$ value.

Table 2. Measuring asymmetry in the J_ℓ^3 with K . The three North poles that maximise the asymmetry for WMAP, and the fraction of simulations with a lower value of $|K|_{max}$.

$\ell = 4 - 150$	
(57,10)	0.808
(63.9,20)	0.707
(85.1,20)	0.689
$\ell = 4 - 100$	
(57,10)	0.994
(63.9,20)	0.946
(40,0)	0.832
$\ell = 4 - 50$	
(63.9,20)	0.988
(57,10)	0.922
(40,0)	0.916

We observe significant asymmetry at the $\sim 99\%$ level for both ℓ ranges 4-100, and 4-50. The North pole positions that maximise this asymmetry differ slightly between the ℓ ranges, but both are consistent with the (57,10) position that Eriksen & al (2004a) found maximises the angular power spectrum asymmetry. Furthermore, the pattern on the sky displayed in Fig. 6 is very similar to that for the distribution of power, see Fig. 24 in Hansen, Banday & Górski (2004).

Whether this anomaly is a sign of anisotropy, non-Gaussianity or both is partly rhetorical. An anisotropic ensemble may always be converted into an isotropic one by randomising the preferred axis. From the point of view of such an ensemble, what appears in a single sky as a sign of anisotropy is simply non-Gaussianity (see Ferreira & Magueijo (1997) for details).

As previously mentioned, for a Gaussian random field the normalised bispectrum and the power spectrum are independent quantities. In the analysis in this section we were particularly careful to avoid selection effects (we let Gaussian simulations choose their maximal asymmetry axis). Should one insist that the anomaly found is a fluke, however, we should stress that it would be an independent fluke with respect to the anomaly found in the power spectrum (Eriksen & al 2004a). This makes it even more unlikely. We shall return to this matter in Section 6.

4.2 Single- ℓ normalised bispectrum

We calculate the single- ℓ normalised bispectrum, I_ℓ^3 , on the Northern and Southern hemispheres for a North pole at $(\ell, b) = (57, 10)$. In Fig. 7 we plot them against each other, and against the whole sky results. We also plot the 1 sigma error bars for the whole sky (the spread is very similar for a half-sky). The Northern results appear to fluctuate more widely than the Southern, and to investigate this further we calculate the χ^2 values for both hemispheres, for various ℓ ranges.

In Table 3 we show the fraction of simulations that find lower χ^2 values, with our simulations also using a North pole at (57,10). The WMAP Northern χ^2 values are consistently high, while the Southern are low. For $\ell = 2-100$ the Southern χ^2 is low at the 99% level. However, the significance of this

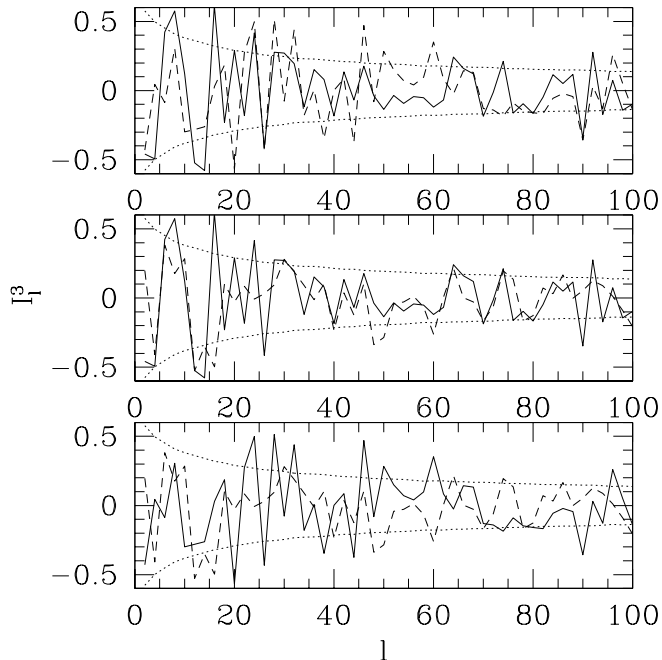


Figure 7. The I_ℓ^3 spectra: top panel, allsky (bold) and Northern (dashed); middle panel, allsky (bold) and Southern (dashed); bottom panel, Northern (bold) and Southern (dashed).

Table 3. Measuring asymmetry in the I_ℓ^3 with χ^2 . The fraction of simulations which have a lower χ^2 for the South, a lower χ^2 for the North, and a lower ratio of the two.

l range	S	N	N/S
2-200	0.10	0.88	0.96
2-150	0.03	0.91	0.99
2-100	0.01	0.88	0.99
32-62	0.14	0.88	0.95
2-50	0.12	0.95	0.97
2-40	0.07	0.83	0.96

asymmetry is not seen in these individual values from the North and the South, but in the ratio of the two: the fact that one is low *while* the other is high. Therefore, in Table 3 we also record the fraction of simulations which find a lower ratio, $\text{MAX}(\frac{\chi_N^2}{\chi_S^2}, \frac{\chi_S^2}{\chi_N^2})$.

Our I_ℓ^3 asymmetry appears significant at the 99% level for a North pole at (57,10). However, we must take account of our North pole selection as we may have pre-selected the North pole that maximises this asymmetry while we have not done the same for the simulations. As before, we vary the North pole position for the WMAP and for the simulations through a further 53 positions that are uniformly distributed in the Northern galactic hemisphere (and infer the results for the positions on the Southern galactic hemisphere). At every North pole position we calculate χ_N^2/χ_S^2 , and χ_S^2/χ_N^2 , and for each simulation we record the maximum chi-squared ratio result from all these values. In Table 4 we record the North pole positions which maximise the ratio for the WMAP data, and the fraction of simulations with lower maximum ratio values. We visualise this in Fig. 8.

Table 4. Measuring asymmetry in the I_ℓ^3 with the North-South χ^2 ratio. The fraction of simulations which, when varying the North pole, find a lower maximum ratio.

$\ell = 2 - 150$	
(57,10)	0.581
(340.5,20)	0.180
(149.0,20)	0.108
$\ell = 2 - 100$	
(180,0)	0.683
(57,10)	0.527
(149,20)	0.431
$\ell = 2 - 50$	
(0,20)	0.940
(340.5,20)	0.587
(21.3,20)	0.557

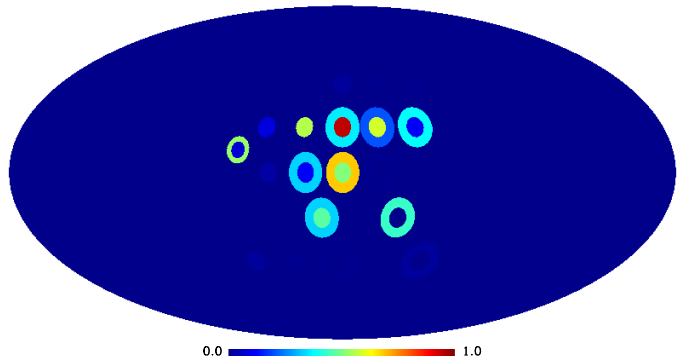


Figure 8. Asymmetry in the I_ℓ^3 with the N-S χ^2 ratio. Fraction of simulations with a lower maximum ratio.

The significance of our asymmetry detection in the single- ℓ bispectrum has weakened greatly now that we have taken a selection effect into account. In fact the only hint of asymmetry that survives is at a level of 94%, for the range $\ell = 2-50$ with North pole at (70,0). This result is not significant enough to rule out Gaussianity. In Fig. 8 we see that very few positions have a chi-squared ratio comparable to the simulations' maxima. Further, those that do, group together towards the galactic centre. This is a very different pattern from that observed for the inter- ℓ bispectrum asymmetry, implying that any asymmetry here is unrelated. The grouping towards the galactic centre does raise some concern that the mask or foreground contamination may have a subtle effect on the single- ℓ bispectrum.

4.3 3-point correlation function

We briefly comment on the three-point correlation function, $C^{(3)}(\theta)$, and its asymmetry reported by Eriksen & al (2004a). We refer to this work for a direct definition (in position space) of $C^{(3)}(\theta)$. The $C^{(3)}(\theta)$, is related to our

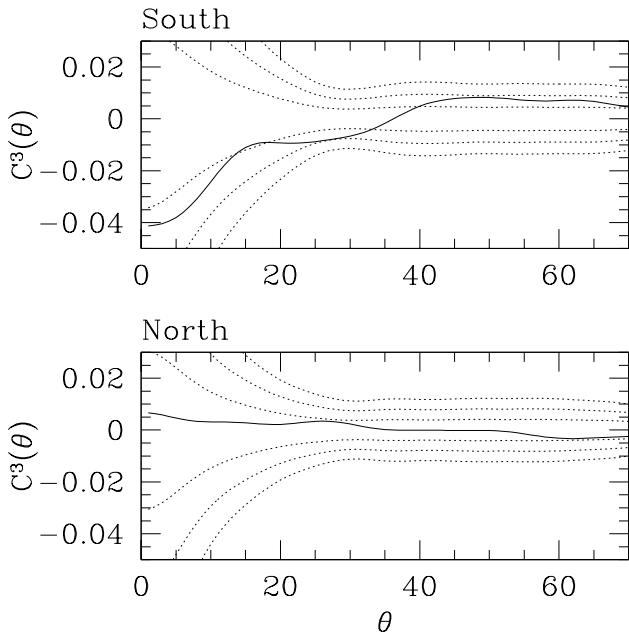


Figure 9. The threepoint correlation function, $C^{(3)}(\theta)$ in $10^6(\mu K)^3$, from the Northern and Southern ecliptic hemispheres, with 1,2 and 3 sigma error bars from simulations.

definition of the bispectrum $\hat{B}_{\ell_1\ell_2\ell_3}$, by

$$\begin{aligned}
 C^{(3)}(\theta) &= \sum_{\ell_1\ell_2\ell_3} \hat{B}_{\ell_1\ell_2\ell_3} P_{\ell_3}(\cos(\theta)) \times \\
 &\quad \left(\begin{array}{ccc} \ell_1 & \ell_2 & \ell_3 \\ 0 & 0 & 0 \end{array} \right)^2 \frac{(2\ell_1+1)(2\ell_2+1)(2\ell_3+1)}{(4\pi)^{\frac{3}{2}}} \\
 &\equiv \sum_{\ell_1\ell_2\ell_3} X_{\ell_1\ell_2\ell_3} P_{\ell_3}(\cos(\theta))
 \end{aligned} \tag{8}$$

It is computationally advantageous to calculate $C^{(3)}(\theta)$ in Fourier space – through this summation – than directly over all points in the sky. Initially, we follow Eriksen & al (2004a) and choose not to include the dipole and quadrupole terms, because of their well known anomalous behaviour; therefore we perform the summation in equation (8) for $\ell \geq 3$.

In Fig. 9 we plot the results from the Northern and Southern *ecliptic* hemispheres (scaled by their respective areas), with 1,2 and 3 sigma error bars from simulations. As can be appreciated from these plots, we have confirmed the findings of Eriksen & al (2004a): a featureless $C^{(3)}(\theta)$ in the Northern ecliptic hemisphere. It is unlikely, however, that this result is simply related to the bispectrum asymmetry reported in Section 4.1, as we shall now argue.

The three-point correlation function is a function in *real* space, while the bispectrum and power spectrum are in *Fourier* space. It is often not intuitively clear how a feature in one will manifest itself in the other. The $|X_{\ell_1\ell_2\ell_3}|$ values decrease very quickly with increasing ℓ , so it is the earliest values that contribute the most, and determine the overall shape of $C^{(3)}(\theta)$. Including $\ell \geq 8$ terms returns $C^{(3)}(\theta)$ values approximately an order of magnitude less than when including $\ell \geq 2$ terms. Therefore, an effect that looks to propagate through a large range in real space, could be from a

Table 5. Excluding lower ℓ contributions in the calculation of $C^{(3)}(\theta)$. The fraction of simulations that found a lower χ^2 from the Northern and Southern ecliptic hemispheres.

Min ℓ	χ_N^2	χ_S^2
2	0.066	0.716
3	0.125	0.912
4	0.068	0.521
5	0.074	0.442
6	0.000	0.601
7	0.020	0.724
8	0.009	0.687

small number of values at this low- ℓ end in Fourier space. Taking this into account could decrease the significance of such a detection of asymmetry. In light of current uncertainties about foreground contamination in the low- ℓ multipoles (Slosar & Seljak 2004; Bielewicz, Górski & Banday 2004; Hansen, Banday & Górski 2004) we investigate if the asymmetry survives when we exclude low- ℓ contributions.

We repeat the calculation of $C^{(3)}(\theta)$ on the Northern and Southern hemispheres, and each time we increase the minimum ℓ value allowed to contribute, *i.e.*, start the summation in equation (8) from an increasing minimum ℓ value. We do the same for our simulations. For each computation, we perform a reduced chi-squared analysis over the θ range $[0,70]$, and in Table 5 we record the fraction of ~ 500 simulations that find a lower χ^2 value than the Northern and Southern WMAP results. Our simulations also use the ecliptic poles. We stress that we are not interested in the level of significance of this anomaly (we have not accounted for selection effects), but how the significance changes as we exclude low- ℓ terms. We find the asymmetry does not diminish as we exclude the lower- ℓ contributions, implying an asymmetry that is a widespread feature in ℓ space.

We emphasize that this asymmetry is different to that explored above with I_ℓ^3 and J_ℓ^3 , as here we are not independent of the power spectrum.

5 THE QUADRUPOLE

The geometrical meaning of the bispectrum becomes clearer by focusing on the quadrupole. Also, the low value of the WMAP quadrupole has inspired much speculation; our remarks shed some light on this matter.

In general a given multipole may be decomposed into the angular power spectrum C_ℓ (the radius) and an axis (a direction), in $2\ell + 1$ dimensions. Alternatively the latter may be represented as ℓ independent unit vectors in 3 dimensions (Copi, Huterer & Starkman 2003; Schwarz & al 2004). These contain the remaining 2ℓ degrees of freedom (d.o.f); but given that there are 3 rotational d.o.f. in the choice of the coordinate frame (and that each multipole is an irreducible representation of the rotation group), such vectors cannot be rotationally invariant, *i.e.* they depend on the way the system of coordinates was set up.

For instance the quadrupole has a total of 5 d.o.f. One is C_2 , so there is only one other invariant. The 2 3D axes resulting from the procedure in Copi, Huterer & Starkman (2003) contain all the remaining 4 degrees of freedom, so they mix

Table 6. The Quadrupole bispectrum and eigenvectors; and some “unusual directions”.

Dataset	I_2^3	\mathbf{v}_1		\mathbf{v}_2		\mathbf{v}_3	
		l	b	l	b	l	b
Coadd, Kp0	-458	48.01	69.39	-118.43	20.08	149.94	4.48
ILC, Kp0	-439	41.26	63.49	-115.40	24.60	150.32	9.25
ILC	-0.386	-82.66	68.56	66.02	18.54	-20.46	-10.38
Kp0	0.771	-159.78	83.95	172.41	-5.35	82.67	2.80
Dipole	—	-96.15	48.25	—	—	—	—
CTH (Virgo)	—	-110.	60.	—	—	—	—
$\mathbf{w}^{(2,1,2)}$	—	-105.73	56.62	—	—	—	—

the issues of non-Gaussianity and anisotropy. In fact there are three independent aspects to quadrupole anomalies: the low value of the angular power spectrum (C_2), its possible non-Gaussianity, and its possible anisotropy.

An alternative approach is that pioneered in Magueijo (1995) (the two approaches actually coincide for $\ell = 1$). By rewriting the spherical harmonics in Cartesian coordinates (instead of their more popular rendition in polar coordinates) one obtains a symmetric multilinear form of order ℓ . Thus the ℓ multipole may be regarded as a traceless, symmetric, rank ℓ tensor. From this one may extract $2\ell - 2$ (invariant) contractions, and a orthonormal frame. For example the quadrupole may be regarded as a 3×3 symmetric traceless matrix. By considering Cartesians $x^i = (z, x, y)$ (with constraint $x^2 + y^2 + z^2 = 1$) one has:

$$Y_0^2 = \sqrt{\frac{5}{16\pi}}(2z^2 - x^2 - y^2) \quad (9)$$

$$Y_{\pm 1}^2 = \mp \sqrt{\frac{15}{8\pi}}(x \pm iy)z \quad (10)$$

$$Y_{\pm 2}^2 = \sqrt{\frac{15}{32\pi}}(x \pm iy)^2 \quad (11)$$

Thus the quadrupole may be rewritten as

$$\delta T_2 = \sum_m a_{2m} Y_{2m} = Q_{ij} x^i x^j \quad (12)$$

leading to matrix

$$Q_{ij} = \sqrt{\frac{5}{16\pi}} \begin{pmatrix} \frac{2a_{20}}{\sqrt{3}} & -\sqrt{2}a_{21}^{re} & \sqrt{2}a_{21}^{im} \\ -\sqrt{2}a_{21}^{re} & -\frac{a_{20}}{\sqrt{3}} + \sqrt{2}a_{22}^{re} & -\sqrt{2}a_{22}^{im} \\ \sqrt{2}a_{21}^{im} & -\sqrt{2}a_{22}^{im} & -\frac{a_{20}}{\sqrt{3}} - \sqrt{2}a_{22}^{re} \end{pmatrix} \quad (13)$$

The 5 d.o.f. in this matrix split into 2 invariants and the 3 d.o.f. associated with coordinate axes’ orientation; for example 2 independent eigenvalues (the 3 eigenvalues must add to zero) and 3 orthonormal eigenvectors. The two invariants may also be the square of the matrix (the sum of the squares of its eigenvalues) and its determinant (the product of the eigenvalues). The first invariant is the power spectrum, the latter the bispectrum. However for a Gaussian these are not statistically independent, since in 3D they must satisfy the constraint

$$|\det Q| \leq \frac{Q^3}{3\sqrt{6}} \quad (14)$$

Thus, one should consider the normalised bispectrum, here rewritten as:

$$I_2^3 = \frac{3\sqrt{6} \det Q}{Q^3} \quad (15)$$

if we want to separate power spectrum effects from non-Gaussianity issues. The variables C_2 , I_2^3 , and the vector system are now independent random variables; C_2 has a χ_5^2 distribution, I_2^3 a uniform distribution in $[-1, 1]$, and the eigenvectors are uniformly distributed.

The issues of isotropy and non-Gaussianity are now fully separated. We have checked with Monte Carlo simulations that indeed I_2^3 and the eigenvectors are uniformly distributed when considering a Gaussian as seen through WMAP. Do the quadrupole eigenvectors point in a suspicious direction? We plot results in Table 5, for the inverse noise squared coadded map, with Kp0 mask, for the internal linear combination map with and without the Kp0 mask, and for the mask alone. None of the eigenvectors appears to correlate with the kinematic dipole direction, with the directions spotted by Schwarz & al (2004), or with those found by Oliveira-Costa & al (2004) (which is roughly in the direction of the Virgo cluster).

We conclude that the bispectrum analysis provided in this paper does not show anything abnormal for the quadrupole.

6 DISCUSSION: SELECTION EFFECTS AND “ANOMALIES”

In the bispectrum studies above we were very conservative about selection effects. For instance, the flat patch found in Section 3 was dismissed on the grounds that any Gaussian realization will reveal a flat patch *somewhere* if a sufficiently long string of ℓ s is considered (a similar argument did not degrade the detection in Section 4). We stress that the flat patch effect may be real if we take a closer look at selection effects, the meaning of anomalies and the role of priors.

“Anomaly”: the very name conjures images of prejudice. And yet, it’s extremely difficult to make statistical statements without an a priori expectation. This expectation defines the “non-anomalous” model. But if the model makes a large number of statistical predictions, looking into a sufficient number of observations will eventually turn out an anomaly even if the model is right. Using this argument we rejected the flat patch described in Section 3. However, it could also be that the anomaly is real, and is in fact a vindication of an alternative model. In this case our choice

of prior and subsequent classification of the anomaly as a fluke has dramatically prejudiced the analysis.

An interesting historical example is the flat patch found in the COBE-DMR four year data (Magueijo 2000). Taken on its own it could not be dismissed as a selection effect (it covered most of the range to which the experiment was sensitive). If WMAP had confirmed a flat patch in the COBE range ($\ell = 4 - 20$) but not elsewhere, then we would have the strange result that *more* data would *decrease* the significance of a detection. This obviously means that we have excessively favoured a Gaussian prior.

More interesting is what actually happened: WMAP failed to confirm the COBE flat patch. This showed that indeed the observed COBE flat patch was *not* a fluke: it was a systematic. Magueijo & Medeiros (2003) explained in detail the origin of the systematic error.

The rejection of the flat patch described in Section 3 as a selection effect could be a further example of the dangers of blind use of a Gaussian prior. Let us consider a simplified model in which N is the number of observed independent bispectrum components and p be the probability that each one of them is within n sigma of the mean. If we define a flat patch with $n = 1$ we have $p \approx 0.68$. The probability of a flat patch longer than L starting at a given fixed multipole is p^L . In WMAP a flat patch occurs with length $L = 16$, starting at $\ell = 32$. Its probability for a Gaussian is $p_L = 0.002$, seemingly ruling out Gaussianity.

In Section 3 we argued that a selection effect was at play. Using our simplified model, the probability of a Gaussian generating a flat patch longer than L starting *anywhere* is $p^L(N - L + 1)$. In this case, considering that $N \approx 100$ (number of signal dominated bispectrum components), we get a probability 0.18, i.e. consistency with Gaussianity. In Section 3 we refined this argument with Monte Carlo simulations.

The problem with this argument is that it is reversed if there is a theory predicting a flat patch in the range $\ell = 32 - 62$, and this is used as a prior. Then Gaussianity is ruled out at the 99.6% confidence level. So the prior is all important. As the example of COBE-DMR shows the threat of systematics should make us beware of simply dismissing anomalies as flukes.

We stress that none of these remarks apply to the results in Section 4.1, concerning North-South asymmetries in the normalised inter- ℓ bispectrum. We were particularly careful to compare like with like - letting the Gaussian simulations choose the axis of maximal symmetry, just as we did with the data. The fact that the maximal asymmetry axis correlates well with that found for the power spectrum asymmetry reinforces the detection. For a Gaussian process power spectrum and normalised bispectrum are independent random variables: one would need two independent flukes instead of one.

7 SUMMARY

In this paper we have performed tests of Gaussianity and explored possible asymmetries of the WMAP first year data. We calculated the inter- ℓ , J_ℓ^3 , and single- ℓ , I_ℓ^3 , normalised bispectrum and compared the WMAP results with those from simulations. We found the whole sky results to be con-

sistent with Gaussianity, barring a 'flat patch' anomaly in the I_ℓ^3 for $\ell = 32 - 62$. Depending on our attitude toward priors this may or may not be seen as rejecting Gaussianity at the 99.6% confidence level.

We also searched for hemisphere asymmetries in the bispectrum, and using the J_ℓ^3 found a North-South asymmetry, with significance level maximised at 99% for a North pole at $(\ell, b) \approx (57, 10)$. This is the same North pole that maximises angular-power spectrum asymmetry (Eriksen & al 2004a; Hansen, Banday & Górski 2004). A similar analysis with I_ℓ^3 showed consistency with Gaussianity.

We noted that asymmetries in the 3-point correlation function, $C^3(\theta)$, (Eriksen & al 2004a) do not diminish when one excludes low- ℓ contributions. However such asymmetries are unlikely to be related to those reported in this paper. Our quadrupole analysis failed to find any correlation with previously reported anomalies (Schwarz & al 2004; Oliveira-Costa & al 2004).

Whether these features are real or the hallmark of further systematic errors remains to be seen.

ACKNOWLEDGEMENTS

We would like to thank A.J. Banday, M. Kuntz and J. Medeiros for help with this project. The results in this paper have been derived using the HEALPix package (Górski, Hivon & Wandelt 1998).

REFERENCES

- Banday A.J., Zaroubi S., Górski K.M., 1999, astro-ph/9908070
- Bennett C.L. et al., 2003a, *Astrophys. J. Suppl.*, 148, 1
- Bennett C.L. et al., 2003b, *Astrophys. J. Suppl.*, 148, 97
- Bielewicz P., Górski K.M., Banday A.J., 2004, astro-ph/0405007
- Coles P. et al., 2004, *MNRAS*, 350, 983
- Copi C.J., Huterer D., Starkman G.D., 2003, astro-ph/0310511
- Cruz M. et al., 2004, astro-ph/0405341
- Eriksen H.K. et al., 2004, *Astrophys. J.*, 605, 14
- Eriksen H.K. et al., 2004, astro-ph/0401276
- Ferreira P., Magueijo J., 1997, *Phys.Rev.*, D56, 4578
- Ferreira P., Magueijo J., Górski K., 1998, *Astrophys.J.*, 503, 1
- Górski K.M., Hivon E., Wandelt B., 1998, astro-ph/9812350
- Hansen F.K., Banday A.J., Górski K.M., 2004, astro-ph/0404206
- Hansen F.K. et al., 2004, *Astrophys. J.*, 607, 67
- Komatsu E. et al., 2002, *Astrophys. J.*, 566, 19
- Komatsu E., Spergel D.N., Wandelt B.D., 2003, astro-ph/0305189
- Komatsu E. et al., 2003, *Astrophys. J. Suppl.*, 148, 119
- Kogut A. et al., 1996, *Astrophys. J. Lett.*, 464, 29
- Larson D.L., Wandelt B.D., 2004, astro-ph/0404037
- Magueijo J., 1995, *Phys. Lett.*, B342, 32. Erratum-ibid, B352, 499.
- Magueijo J., Ferreira P., Górski K., 1998, astro-ph/9810414
- Magueijo J., 2000, *Astrophys. J. Lett.*, 528, 57
- Magueijo J., Medeiros J., 2003, astro-ph/0311096

Mukherjee P., Wang Y., 2004, astro-ph/0402602
Novikov D., Feldman H., Shandarin S., 1999, Int. J. Mod
Phys, D8, 291
de Oliveira-Costa A. et al., 2004, Phys. Rev, D69, 063516
Park C., 2004, MNRAS, 349, 313
Sandvik H., Magueijo J., 2001, MNRAS, 325, 463
Schwarz D. et al., 2004, CERN-PH-TH/2004-052
Slosar A., Seljak U., 2004, astro-ph/0404597
Spergel, D.N. and Goldberg, D.M., Phys.Rev. D59, 103001,
1999
Vielva P. et al., 2003, astro-ph/0310273

This paper has been typeset from a $\text{T}_{\text{E}}\text{X}/\text{L}^{\text{A}}\text{T}_{\text{E}}\text{X}$ file prepared
by the author.